Electronic Supplementary Material (ESI) for ChemComm.

Self-Assembly of a Si-based Cage by the Formation of 24 Equivalent Covalent Bonds

Jessica L. Holmes,[a] Brendan F. Abrahams,[a] Anna Ahveninen,[a] Berin A. Boughton,[b] Timothy A. Hudson,[a] Richard Robson[a] and Dinaiz Thinagaran[b]

Electronic Supporting Information

a School of Chemistry, University of Melbourne, Parkville, Victoria 3010, Australia

b Metabolomics Australia, School of Biosciences, University of Melbourne, Parkville, Victoria 3010, Australia

S1. Comments on the formulation of the cage

The covalent anionic tetrahedral cage has the formula $[(PhSi)_6(ctc)_4]^{6-}$. Whilst single crystal X-ray diffraction clearly revealed the structure and formula of the cage, other techniques have been employed to identify counterions, tetraethylammonium, triethylammonium and bromide. For example, NMR has been used to determine that the cage forms as a DMF/EtOAc solvate (see *S5. NMR spectroscopy*). The amount of solvent present varies depending on the treatment of the crystals; water is incorporated when the crystals are exposed to the atmosphere for extended periods of time.

S2. Instrumentation

Microwave reactor synthesis of the compound was performed using a Biotage Initiator Classic microwave reactor. Single crystal x-ray diffraction experiments were performed using a SuperNova dual source diffractometer using CuKα radiation λ = 1.5418 Å. Powder X-ray diffraction patterns were measured using a Rigaku Synergy instrument. Mass spectrometry was performed using an Agilent QTOF 6520. High resolution mass spectrometry was performed using a Bruker Daltonics (Bremen, Germany) SolariX 7 Tesla Hybrid MALDI/ESI-FT-ICR-MS. ^{1}H and ^{13}C NMR spectrometry was performed using a Varian 400 MHz NMR Spectrometer. Thermogravimetric analyses were performed using a Mettler TGA/SDTA851 apparatus. Infrared spectroscopy was performed using a Bruker Tensor FTIR 27.

S3. Synthesis and characterisation

Method 1

This method was used for growing crystals for single crystal X-ray diffraction. Preparation of $(NEt_4)_4(HNEt_3)_4[(PhSi)_6(ctc)_4]Br_2$·solvate: Cyclotricatechylene (H_6ctc) (192 mg, 0.52 mmol) was placed in a 10-20 mL microwave vial and dissolved in DMF (6 mL). NEt_4Br (66 mg, 0.31 mmol) in DMF (6 mL) was added to the $ctcH_6$ solution followed by $SiPh(OEt)_3$ (0.30 mL) and excess NEt_3 (ca. 16 drops). The solution was sparged with N_2 for 2 minutes then sealed and placed in a Biotage

Initiator microwave reactor. The solution was heated to 100°C with stirring and held at this temperature for 15 minutes then allowed to cool to room temperature. 2 mL of the reaction mixture was decanted into a vial and exposed to EtOAc vapour for several days over which time large yellow crystals (typical dimensions between 0.5 and 1.0 mm) suitable for x-ray diffraction grew on the surface of the vial. A single crystal was taken from the mother liquor and placed directly into protective oil. Single crystal X-ray diffraction data was collected using a SuperNova diffractometer fitted with a CuKα X-ray source. The X-ray data revealed the crystals to be face centered cubic with the adoption of the space group *F*-43*m*, *a* = 27.9568(6) Å.

In order to improve the yield, reduce solvent usage and reduce crystallization time of the compound the synthetic procedure was modified and the resultant crystalline product used for all further characterization experiments. The method described above is hereafter designated *method 1* and the modified method detailed below is *method 2.*

Method 2

Cyclotricatechylene (192 mg, 0.52 mmol) was placed in a 2-5 mL microwave vial and dissolved in DMF (4 mL). NEt_4Br (66 mg, 0.31 mmol) was then added to the $ctcH_6$ solution followed by $SiPh(OEt)_3$ (0.30 mL) and excess NEt_3 (ca. 16 drops). The solution was sparged with N_2 for 2 minutes then sealed and placed in a Biotage Initiator microwave reactor. The solution was heated to 120°C with stirring and held at this temperature for 30 minutes then allowed to cool to room temperature. The reaction mixture was distributed into 5 vials in equal aliquots before exposure to EtOAc vapour to induce crystallisation. Each aliquot contained 1.05×10^{-5} mol of the limiting reagent, $ctcH_6$.

The crystals formed from method 2 were shown to be the same as those obtained by method 1 by comparison of the powder x-ray diffraction pattern of the product from method 2 with the simulated pattern produced from the crystal structure determination obtained on a crystal produced by method 1 (Figure S5). Crystals from one aliquot were collected via vacuum filtration and dried in a stream of air. These were used for elemental and infrared analyses. Elemental analysis was performed at Campbell Microanalytical Laboratory, Chemistry Department, *Te Tari Hua Ruānuku*, University of Otago. Analysis (air dried sample prepared via

method 2) $(NEt_4)_4(HNEt_3)_4[(PhSi)_6(ctc)_4]Br_2.(DMF)(H_2O)_{19}$: Calc: %C 60.1, %H 7.5, %N 3.5; Found: %C 60.1; %H 6.9; %N 3.3.

Crystals from a second aliquot were collected on a glass frit and washed with minimum EtOAc to measure the yield and ^{13}C (not shown) and ^{1}H NMR spectra of the compound. The percentage yield is based on the best approximation of the chemical formula of vacuum dried crystals $(NEt_4)_4(HNEt_3)_4[(PhSi)_6(ctc)_4]Br_2.4DMF$ (from which all the EtOAc has been removed and have not been exposed to atmospheric water vapour for an extended period of time) as estimated by integration of the ^{1}H NMR spectrum of the dried crystals (see figure S8). The yield was 46.5 mg, 51%.

S4. Further crystallographic details

In the crystal structure investigated, initial refinements involved attempts to assign numerous small peaks of electron density in the difference Fourier maps to atoms of disordered cations and solvent molecules. This approach resulted in unsatisfactorily high agreement values. In response to these difficulties, the SQUEEZE[S1] routine within the crystallographic program PLATON[S2] was used to subtract the contribution of the diffuse solvent from the diffraction data and this led to an improvement in agreement values. It also provided an indication of the volume of the solvent accessible void spaces and the number of electrons in these regions. On the basis of this information as well as thermogravimetric analysis of 'wet crystals' (see *S6 Thermogravimetric analysis*) and ^{1}H NMR (see S5. *NMR spectroscopy*) the number of solvent molecules (assumed to be only DMF and EtOAc) in the unit cell was estimated. Despite the uncertainties arising from the location of solvent molecules and cations within the structure, the anionic cage, which is the focus of our interest, is clearly defined. The formula of the crystal that was crystallographically characterized was assigned as $(NEt_4)_4(HNEt_3)_4[(PhSi)_6(ctc)_4]Br_2{\cdot}(DMF)_4(EtOAc)_6$.

Crystallographic analysis of the crystals immersed in the CsBr solution revealed a similar structure to that of the parent crystals except that a Cs^+ ion was now located in each of the four corners of the $[(PhSi)_6(ctc)_4]^{6-}$ cage. Estimation of the chemical formula of the crystals was difficult because the solvent and cations occupying the inter-cage spaces could not be identified. Given that triethylammonium is likely to be more soluble in water, it was assumed for the purposes of estimating the formula of the crystals that the incorporation of Cs^+ accompanied the loss of

triethylammonium to the aqueous environment upon immersion in the CsBr solution. In addition, it was thought that the dimethylformamide and ethyl acetate would be replaced by water in the crystal. The formula of the immersed crystals therefore was tentatively assigned as $(NEt_4)_4Cs_4[(PhSi)_6(ctc)_4]Br_2{\cdot}70H_2O$. Despite the uncertainty associated with the overall formula, the crystal structure clearly indicates Cs^+ ions associating with the internal surface of the cage.

The cages in both the parent and immersed crystals pack in a face centred cubic (FCC) arrangement in which six phenyl groups from six distinct cages converge upon octahedral sites within the FCC structure as indicated in Fig. S2.

The structures were solved using SHELXT[S3] and refined using a full-matrix least squares procedure based upon F^2 (SHELXL[S4]). The solution and refinement of $(NEt_4)_4(HNEt_3)_4[(PhSi)_6(ctc)_4]Br_2{\cdot}(DMF)_4(EtOAc)_6$was performed within the WinGX system of programs[S5] whereas OLEX2[S6] was employed for $(NEt_4)_4Cs_4[(PhSi)_6(ctc)_4]Br_2{\cdot}70H_2O$.

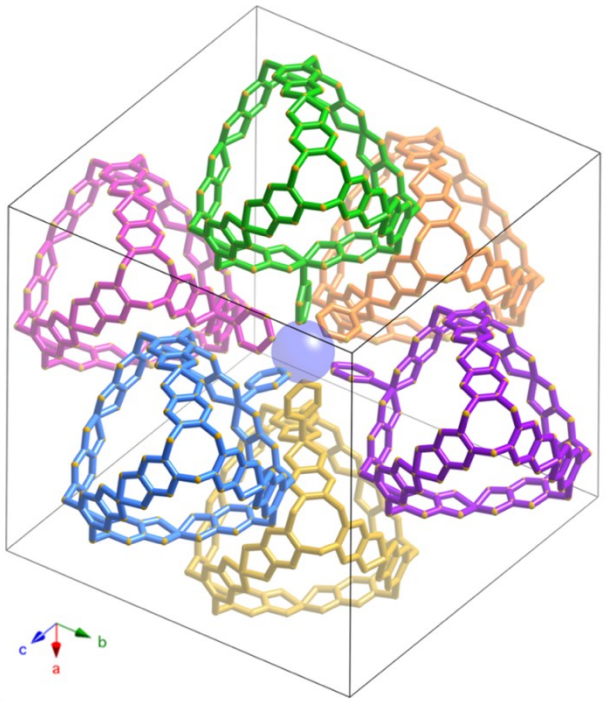

Figure S1 A representation of the packing in $(NEt_4)_4(HNEt_3)_4[(PhSi)_6(ctc)_4]Br_2{\cdot}(DMF)_4(EtOAc)_6$ showing only the cages located in the middle of each face of the cubic unit cell. The translucent sphere corresponds to an octahedral site at the centre of the cell where the phenyl rings from six cages converge. Crystallographically equivalent octahedral sites are located half-way along each edge. Only one phenyl ring from each cage is depicted. The cages located at the vertices of the unit cell are not shown.

S5. NMR spectroscopy

^{1}H NMR spectra were collected for three samples of the compound, each with different post-synthetic treatment. The three samples are shown in Figures S3 and S4. The top sample (3) in each figure corresponds to a sample that was prepared by directly transferring multiple large single crystals directly from the mother liquor into d_6DMSO. The middle sample (2) corresponds to the bulk material collected on a glass frit without suction and washed with ethyl acetate. The bottom spectrum (1) was obtained on the bulk material that was collected on a glass frit and dried at the pump without washing with additional solvent, no heating was performed.

The distinct absence of the three characteristic ethyl acetate peaks (1.18 ppm, 1.98 ppm and 4.03 ppm) in sample 3 shows that it is easily released at room temperature. Aside from this difference, the three spectra have the same peak profile indicating that the bulk sample is the same as the single crystals. A small shift in some of the peaks is observable on loss of ethyl acetate in sample 1.

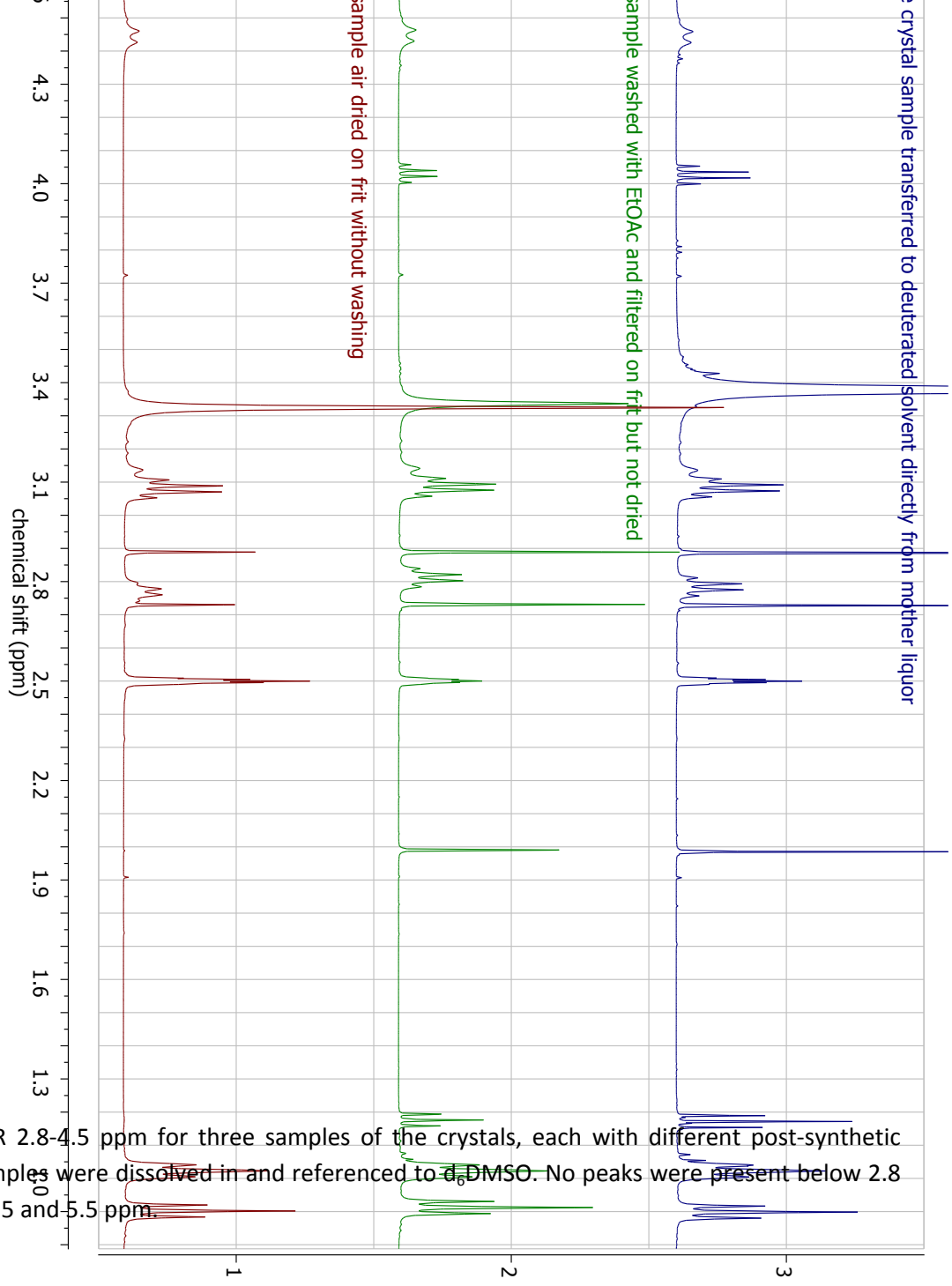

Figure S2. ^{1}H NMR 2.8-4.5 ppm for three samples of the crystals, each with different post-synthetic treatment. All Samples were dissolved in and referenced to d_6-DMSO. No peaks were present below 2.8 ppm or between 4.5 and 5.5 ppm.

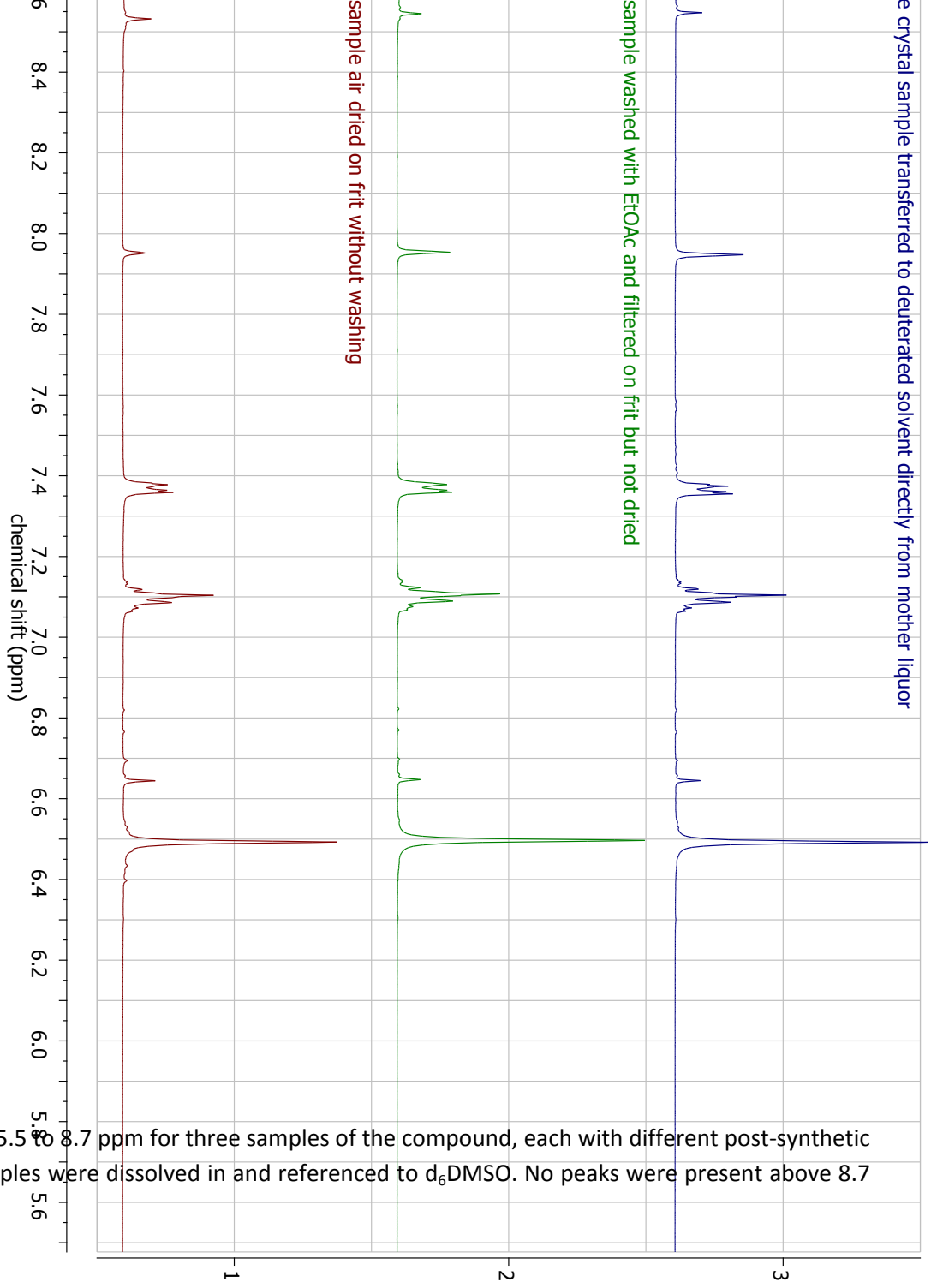

Figure S3. ^{1}H NMR 5.5 to 8.7 ppm for three samples of the compound, each with different post-synthetic treatment. All samples were dissolved in and referenced to d_6DMSO. No peaks were present above 8.7 ppm.

S6. Thermogravimetric analysis

Thermogravimetric analysis (TGA) of two samples of the compound was performed across a temperature range of 25-450 °C. The 'dry crystals', represented below in Figure S5 in blue, were collected on a glass frit and air was pulled through the sample for several minutes. The crystals were left for several days before TGA was performed. Though there is a small initial drop in mass as dry nitrogen was blown across the sample at 25 °C the gradient of the graph remains close to horizontal to temperatures around 250 °C indicating that most ethyl acetate is lost at room temperature. This is confirmed also by ^{1}H NMR of the dried crystals (see S5 Nuclear Magnetic Resonance Spectroscopy). Some of the mass loss below 80 °C may also correspond to water adsorbed from the atmosphere, however this has not been confirmed. The total mass loss up to 450 °C corresponds approximately to all solvent (DMF) and counterions, leaving only the cage remaining. Stability of the cage above 450 °C has not been measured.

The 'wet crystals' were prepared for analysis by filtration on a glass frit in the absence of suction, immediately before being transferred to the TGA instrument. Some solvent loss may have occurred during sample transfer and calibration of the instrument however the steeper gradient of this line indicates presence and subsequent loss of ethyl acetate (and possibly water) up to approximately 250 °C. The TGA data of the wet crystals combined with the NMR provide the basis for the estimate of the chemical formula of the single crystal used for x-ray diffraction, $(NEt_4)_4(HNEt_3)_4[(PhSi)_6(ctc)_4]Br_2{\cdot}(DMF)_4(EtOAc)_6$.

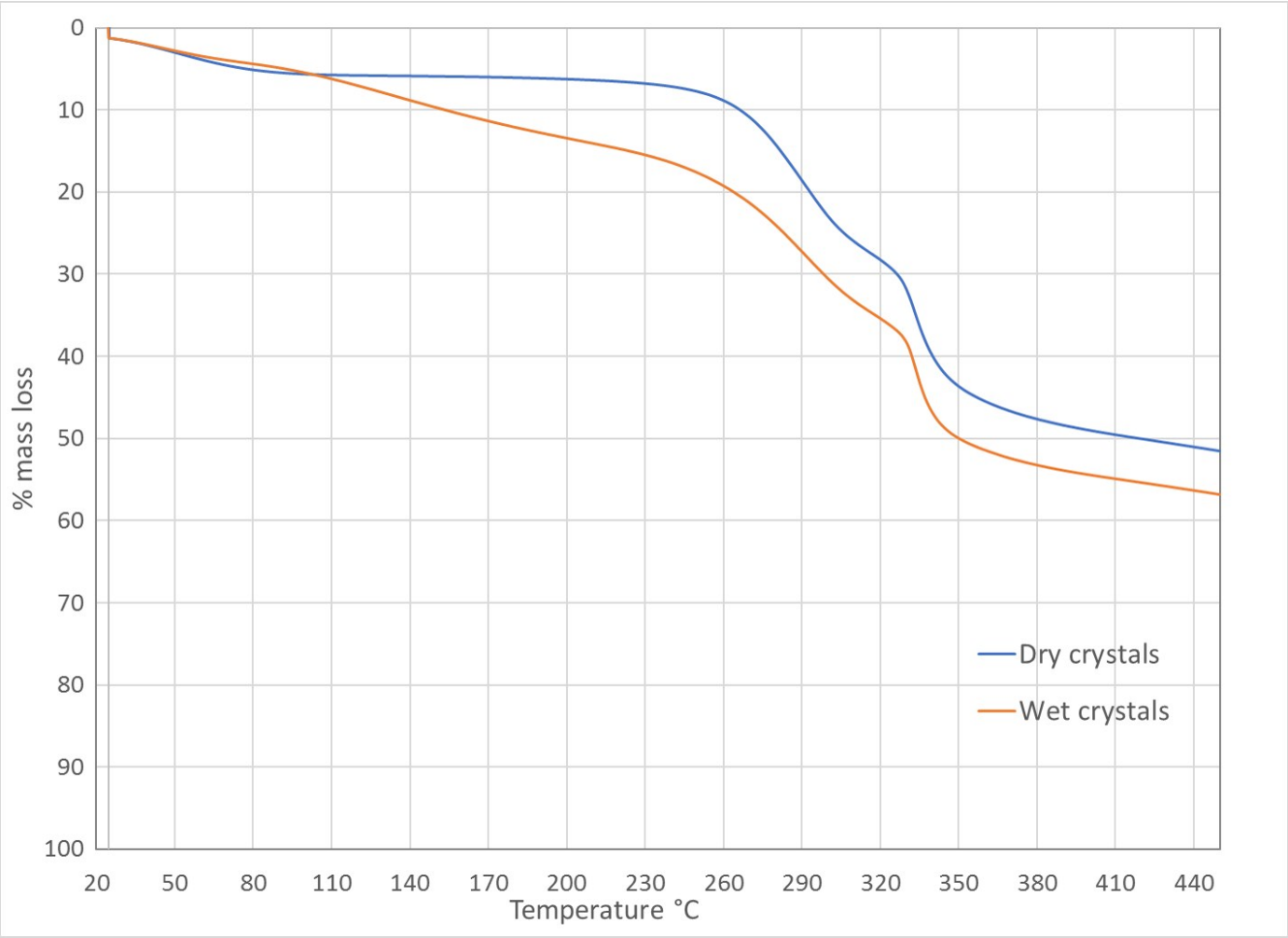

Figure S4. Thermogravimetric traces of air dried crystals that were exposed to atmosphere (blue) and crystals that were collected from their mother liquor with no vacuum and transferred directly to the instrument (red)

S7. Powder Diffraction Patterns

The powder diffraction pattern for the parent compound $(NEt_4)_4(HNEt_3)_4[(PhSi)_6(ctc)_4]Br_2$.solvate (Figure S5), of the boiled crystals (Figure S6) and the crystals soaked in aqueous CsBr (Figure S7) are shown below.

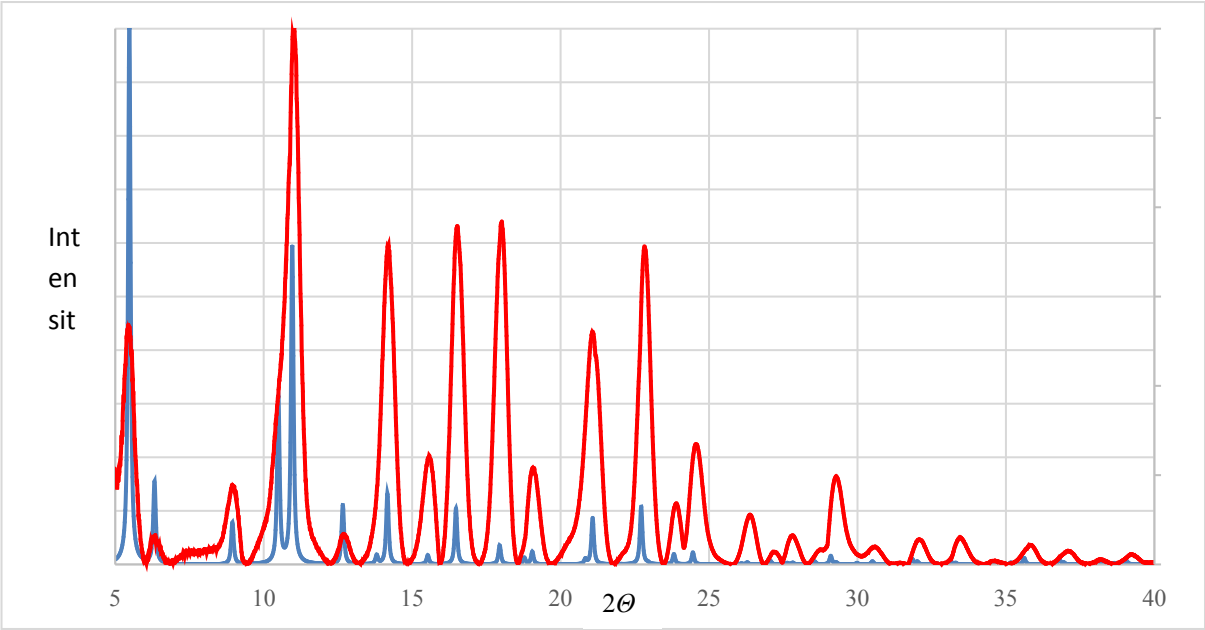

Figure S5. Calculated powder x-ray diffraction pattern of $(NEt_4)_4(HNEt_3)_4[(PhSi)_6(ctc)_4]Br_2$.solvate (blue) compared with experimental data for ground up crystals prepared via *method 2* and washed with a minimum of ethyl acetate (red).

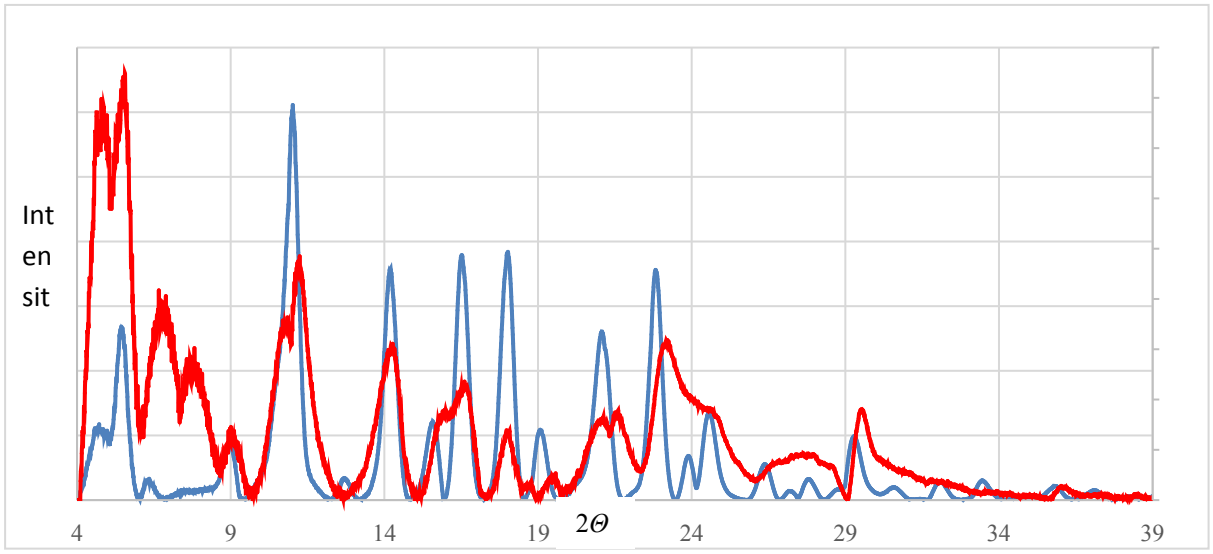

Figure S6. Observed powder diffraction patterns of $(NEt_4)_4(HNEt_3)_4[(PhSi)_6(ctc)_4]Br_2$·solvate untreated (blue) and after being boiled in H_2O for 30 mins (red).

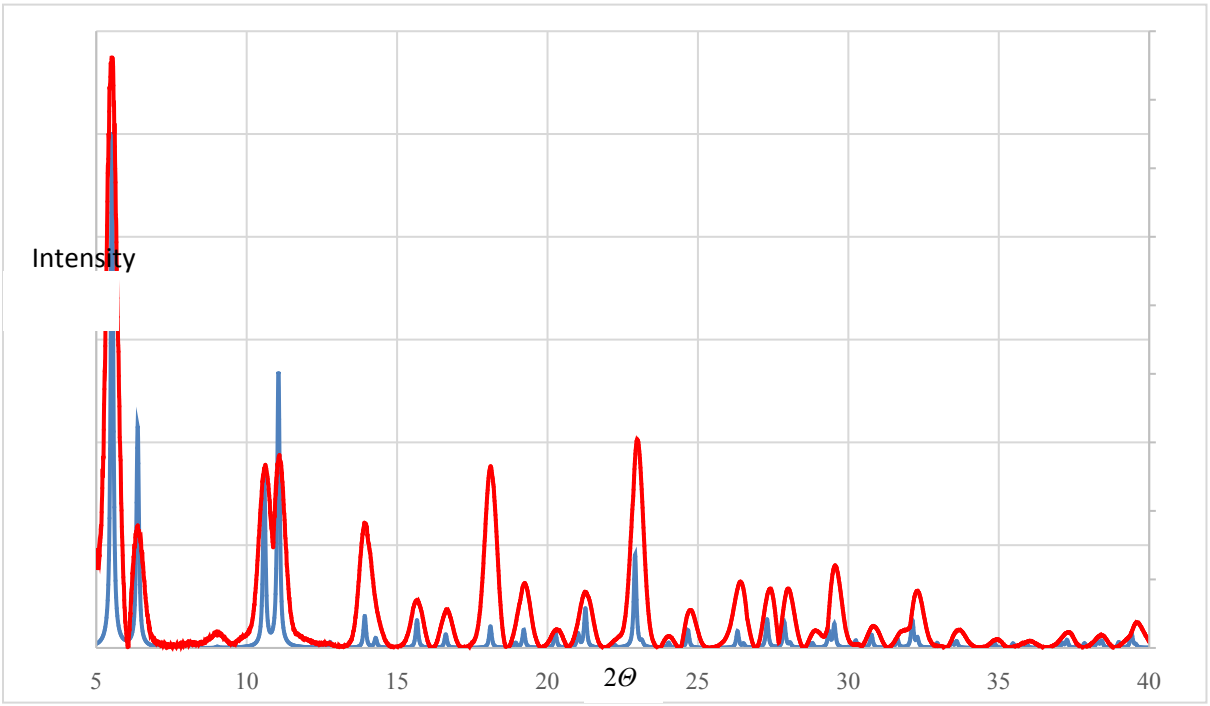

Figure S7. Calculated (blue) and observed (red) powder patterns of the Si-cage crystals, $[(NEt_4)_4Cs_4[(PhSi)_6(ctc)_4]Br_2$·solvate] after immersion in aqueous CsBr.

S8. ESI mass spectrometry

A Bruker Daltonics (Bremen, Germany) SolariX 7 Tesla Hybrid MALDI/ESI-FT-ICR-MS was used for high mass resolution analysis. The instrument was operated in ESI negative and positive ionisation modes with TD acquisition = 1M *m/z* 200-2000 or 4M *m/z* 53.75-3000 providing mass resolutions of 260000 and 140000 at *m/z* 400 respectively, and ESI positive ionization mode. The system was calibrated using an external calibration of ESI-TOF low concentration Tune Mix (Agilent Technologies, Santa Clara, CA, USA). Samples were infused at a rate of 2 µL min^{-1} using the syringe pump, a total of 10-20 scans were collected and averaged to generate mass spectra. The following general instrument conditions were set: capillary voltage, negative mode = 4200 V and positive mode = -4000 V; drying gas flow, 4.0 L min^{-1}; drying gas temperature, 180°C; nebulizer gas flow rate, 1.0 bar; source accumulation, 0.001 sec; ion accumulation, 0.5 sec; ion cooling time, 0.01 sec; flight time, 0.001 sec. Data were analysed using the Bruker Compass Data Analysis 4.2 (Build 383.1) software.

Unless otherwise indicated, the *m/z* values given refer to the base peak of on isotopologue series.

Sample preparation for ESI-MS analysis

1. $(NEt_4)_4(HNEt_3)_4[(PhSi)_6(ctc)_4]$·solvate (untreated crystals)

3-4 large crystals of the compound, prepared via synthetic *method 1*, were dissolved in a minimum of DMF (<1 mL) followed by dilution with acetone (10 mL) prior to analysis.

2. $(NEt_4)_4(HNEt_3)_4[(PhSi)_6(ctc)_4]$·solvate crystals that had been immersed in boiling water

2 mg of crystals of the compound, prepared via synthetic *method 2*, were boiled in deionized water for 30 min then solution was kept at 60°C for 7 days, then filtered, the crystals dried. 3-4 large crystals were dissolved in a minimum of DMSO (<1 mL) followed by dilution with acetonitrile (10 mL).

3. $(NEt_4)_4(HNEt_3)_4[(PhSi)_6(ctc)_4]$·solvate soaked in aqueous CsBr

1 mg of large crystals prepared via synthetic *method 2* was immersed in an aqueous CsBr solution (30 mg in 2 mL water) for 3 days, then filtered and dried. 3-4 large crystals were dissolved in DMF (1 mL) followed by dilution with acetonitrile (10 mL).

Results of ESI-MS analysis

1. $(NEt_4)_4(HNEt_3)_4[(PhSi)_6(ctc)_4]$·solvate (untreated crystals)

Figure S6 shows the full, high resolution ESI mass spectrum in negative mode.

Table S1 lists the dominant isotopologues in the full spectrum. The relative intensities of the base peaks within each of the isotopologue series are indicated as their percentage contribution to the sum of the intensities of the base peaks in each of the isotopologue series. The error (in ppm) for each species is calculated based upon the monoisotopic peak for each isotopologue series.

Figure S7 shows a portion of the spectrum in which a series of dianionic cage adducts are indicated. Figure S8 shows an enlargement of the signal corresponding to [cage + $(NEt_4)_4]^{2-}$ and a comparison with the calculated pattern. An enlargement of the signal corresponding to [cage + $(NEt_4)_3]^{3-}$ and a comparison with the calculated pattern is displayed in Figure S9.

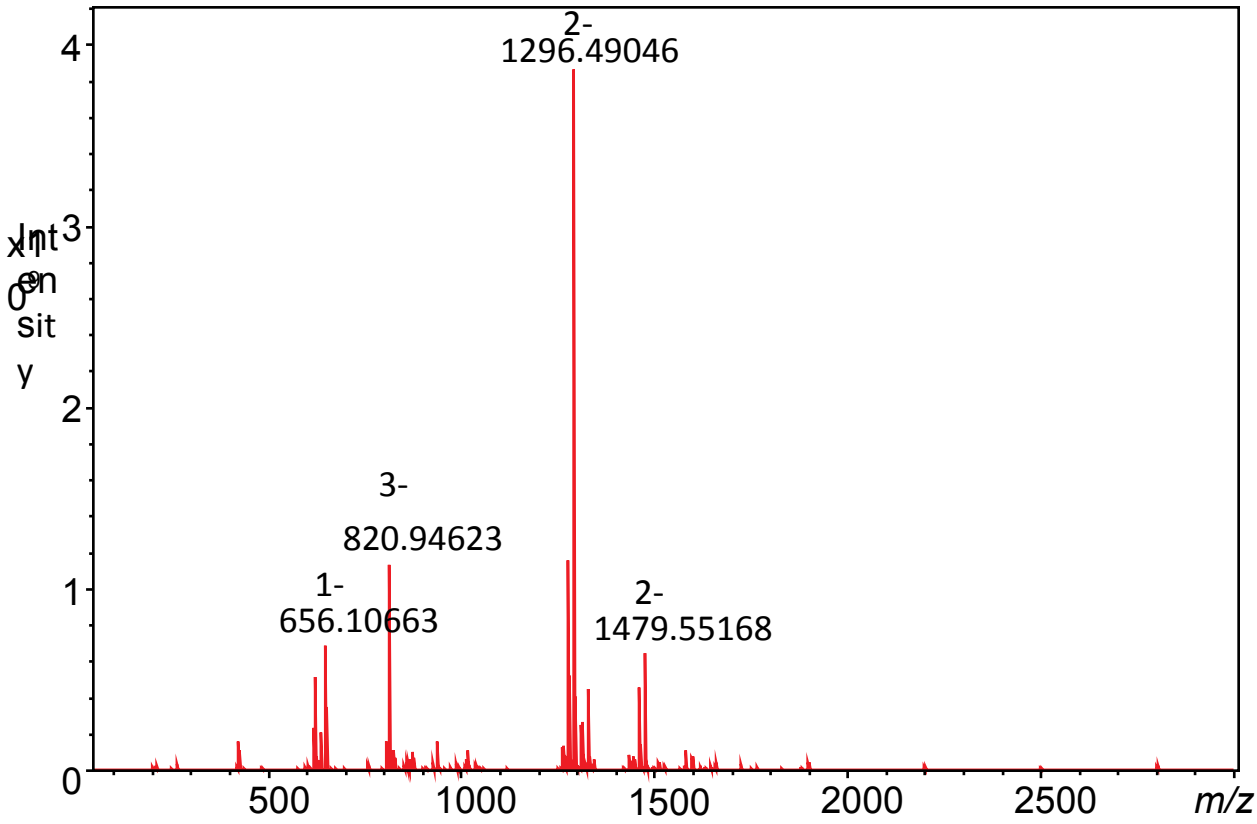

Figure S6. Full ESI-mass spectrum, in negative mode of samples obtained from the dissolution of $(NEt_4)_4(HNEt_3)_4[(PhSi)_6(ctc)_4]$·solvate crystals.

Table S1. Selected negative ionisation mode mass spectrum data for untreated crystals.

m/z (monoisotopic peak)	*m/z* (base peak)	Charge	Species	Mass Error (ppm)	%
626.07767	628.07517	-1		-	4.93
644.02513	644.02513	-1		-	1.98
654.10885	656.10663	-1		-	6.62
810.93470	811.60256	-3	$[cage + (Et_4N)_2(HNEt_3)]^{3-}$	2.12	1.57
820.27857	820.94623	-3	$[cage + (Et_4N)_3]^{3-}$	2.23	10.94
833.20603	833.20603	-1		-	1.04
880.62603	881.62843	-3		-	10.94
942.31547	942.98363	-3		-	1.5
1020.22131	1022.21970	-1		-	1.09
1267.46585	1268.46409	-2	$[cage + (Et_4N)_2(HNEt_3)_2]^{2-}$	1.99	1.29
1281.47736	1282.47689	-2	$[cage + (Et_4N)_3(HNEt_3)]^{2-}$	-1.26	11.08
1295.49110	1296.49046	-2	$[cage + (Et_4N)_4]^{2-}$	-2.72	37
1316.00693	1317.00842	-2	$[cage + (Et_4N)_4 + MeCN]^{2-}$	-0.74	2.59
1332.02091	1333.02389	-2	$[cage + (Et_4N)_4 + DMF]^{2-}$	-0.08	4.33
1332.39625	1333.91475	-2		-	1.41
1464.53513	1465.53452	-2		-	4.36
1478.54996	1479.55168	-2		-	6.2
1583.09263	1584.59398	-2		-	1.04

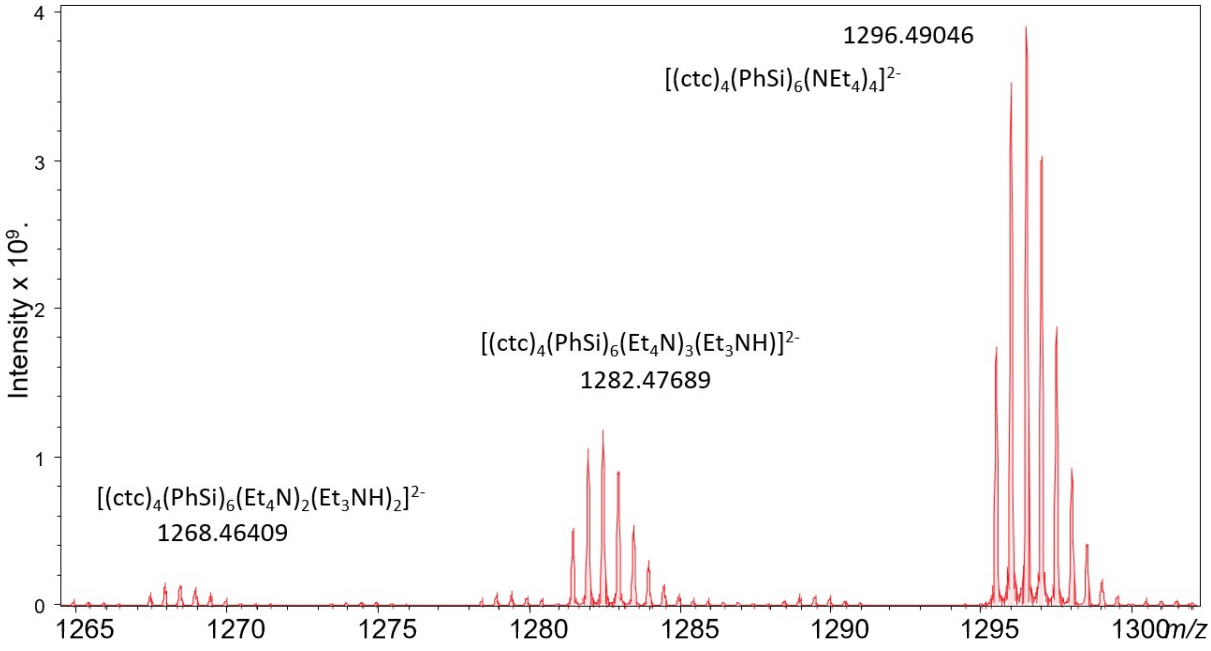

Figure S7. ESI-mass spectrum, in negative mode, of the peaks associated with $[cage + (Et_4N)_4]^{2-}$ at *m/z* 1296.49046, $[cage + (Et_4N)_3 + (Et_3NH)]^{2-}$ at *m/z* 1282.47896 and $[cage + (Et_4N)_2 + (Et_3NH)_2]^{2-}$ at *m/z* 1268.46409 from the dissolution of $[(NEt_4)_4(HNEt_3)_4[(PhSi)_6(ctc)_4]$·solvate crystals.

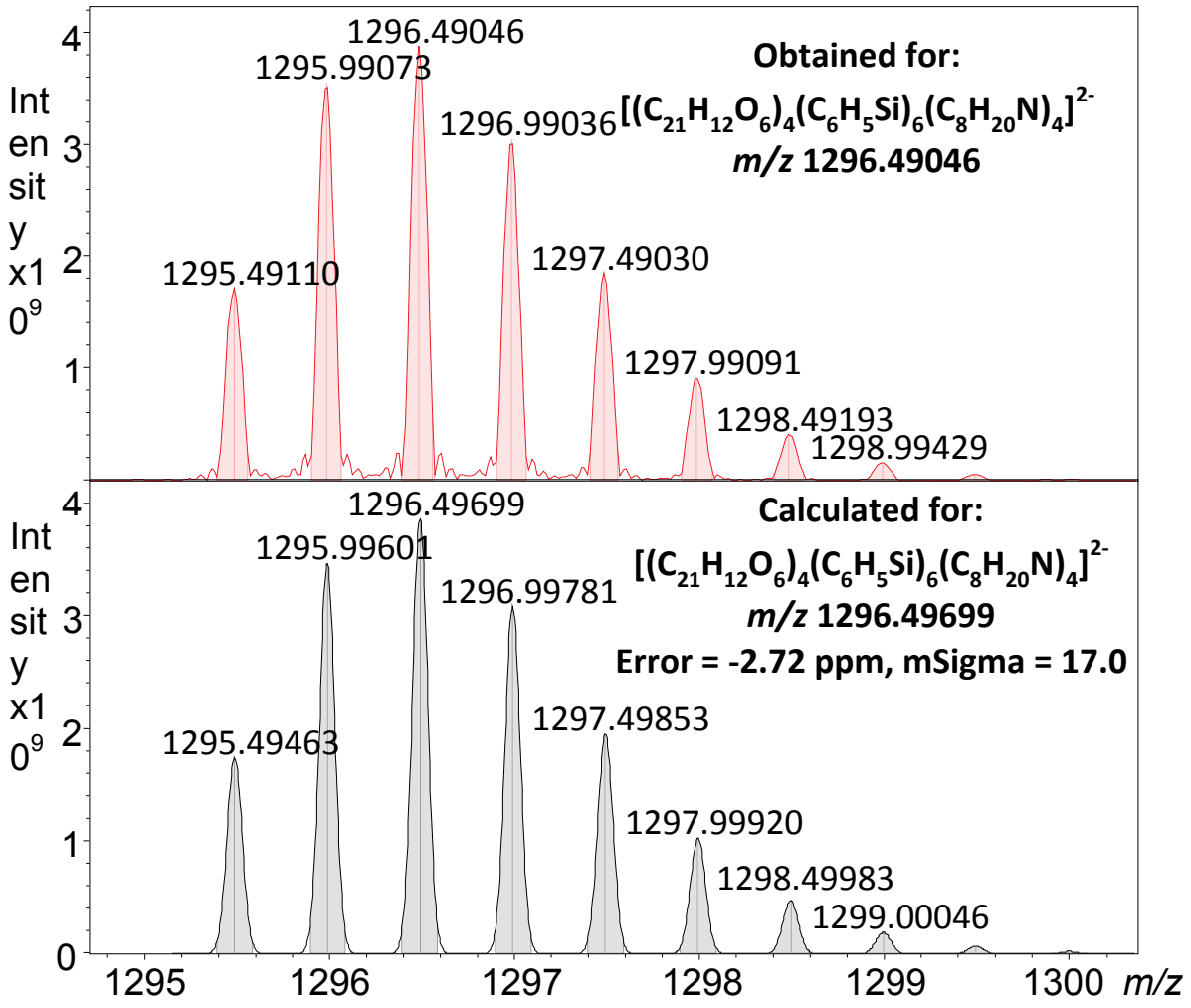

Figure S8. ESI-mass spectrum, in negative mode of the peaks associated with [cage + $(Et_4N)_4]^{2-}$ at *m/z* 1296.49046 from the dissolution of $[(NEt_4)_4(HNEt_3)_4[(PhSi)_6(ctc)_4]$·solvate crystals.

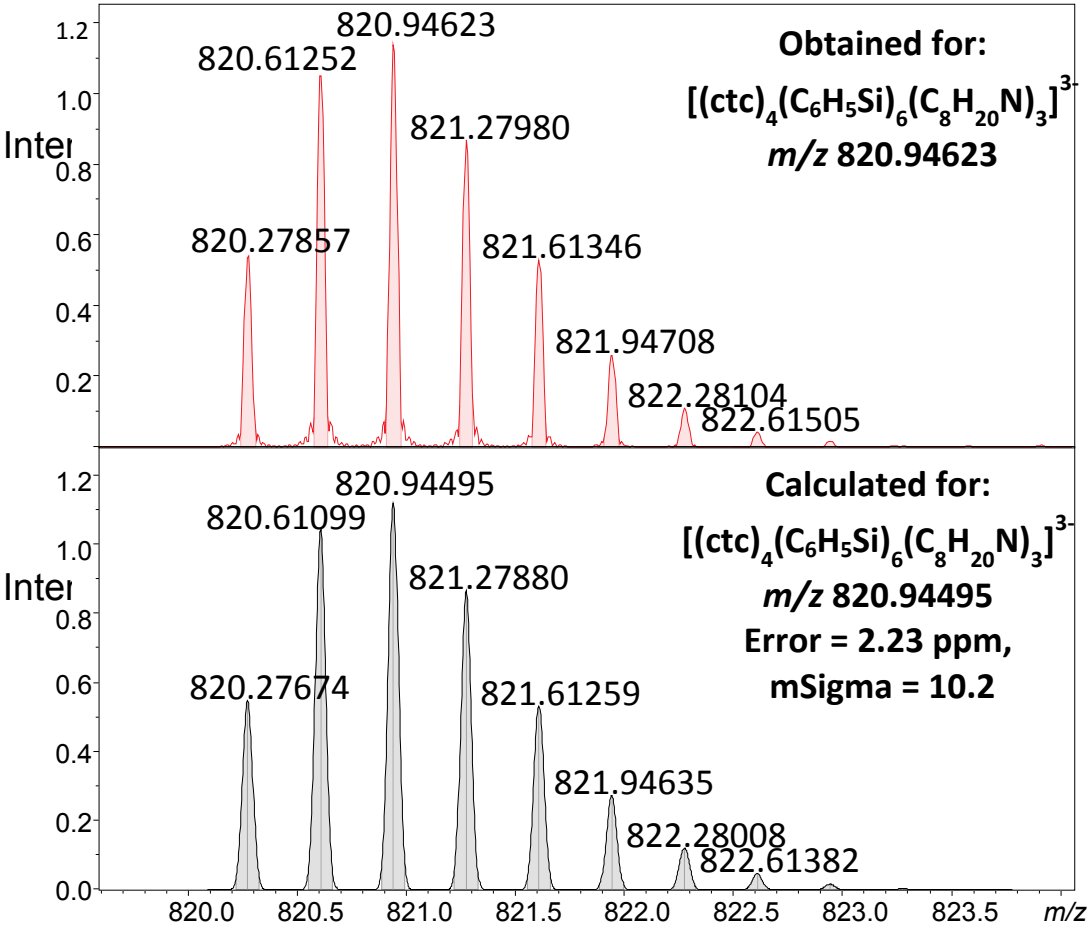

Figure S9. ESI-mass spectrum, in negative mode of the peaks associated with [cage + $(Et_4N)_3]^{3-}$ at *m/z* 820.94623 (base peak) from the dissolution of $(NEt_4)_4(HNEt_3)_4[(PhSi)_6(ctc)_4]$·solvate crystals.

2. $(NEt_4)_4(HNEt_3)_4[(PhSi)_6(ctc)_4]$·solvate crystals that had been immersed in boiling water

Figure S10 shows the full negative mode, high resolution ESI mass spectrum obtained for crystals of the compound boiled in water then dissolved in dimethylsulfoxide and diluted with acetonitrile. The dominant peak in the spectrum corresponds to [cage + $(Et_4N)_3]^{3-}$ at *m/z* 820. 820.94461. Additionally, there is a significant peak corresponding to [cage + $(Et_4N)_2]^{4-}$ at *m/z* 583.16930.

Table S2 lists the dominant isotopologues in the full spectrum. The relative intensities of the base peaks within each of the isotopologue series are indicated as their percentage contribution to the sum of the intensities of the base peaks in each of the isotopologue series. The error (in ppm) for each species is calculated based upon the monoisotopic peak for each isotopologue series.

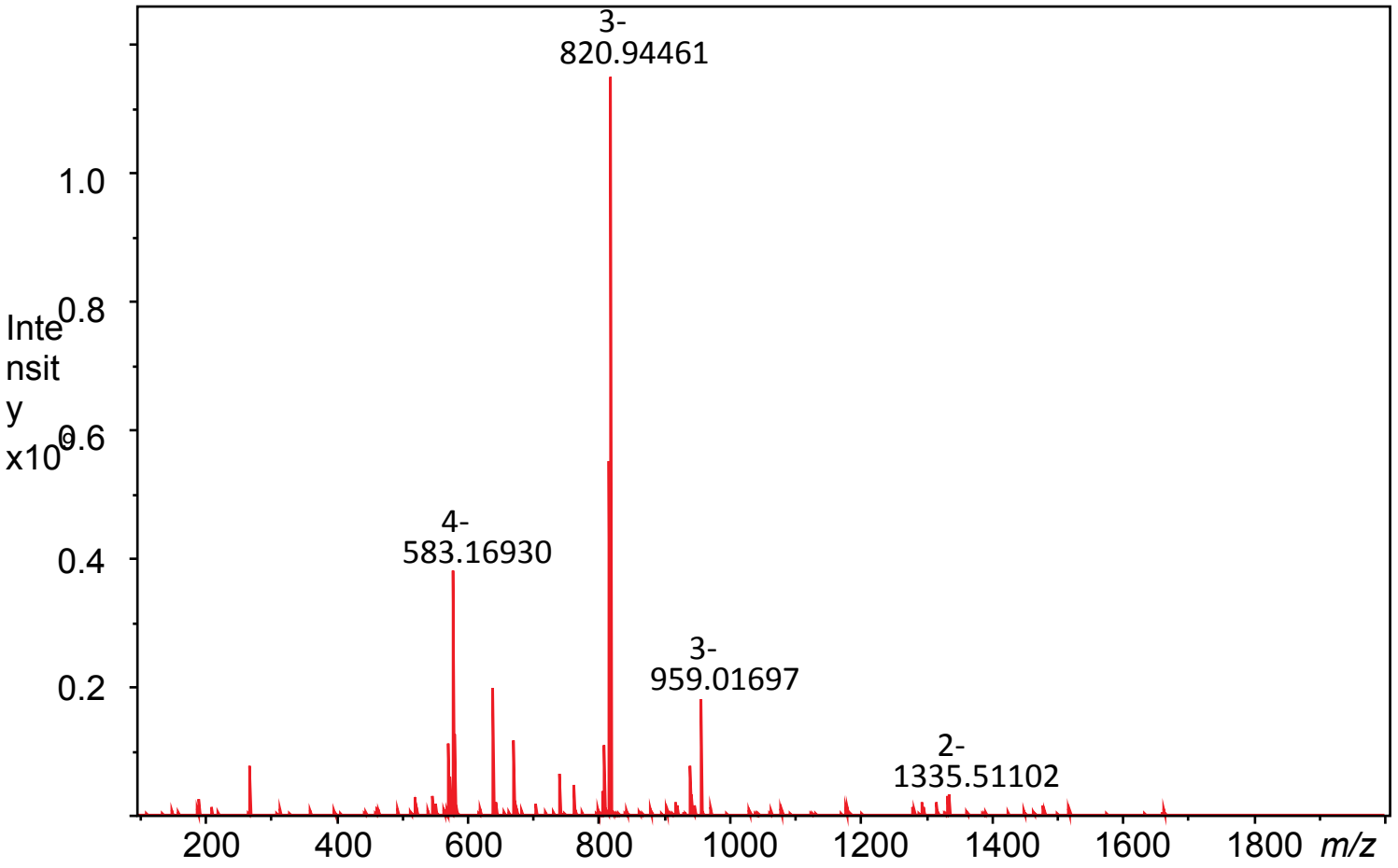

Figure S10. Full negative mode mass spectrum of the crystals that had been boiled in water prior to being dissolved in DMSO and diluted with MeCN.

Table S2. Selected negative ionisation mode mass spectrum data for crystals boiled in water prior to being dissolved in DMSO and diluted with MeCN.

m/z (monoisotopic peak)	*m/z* (base peak)	Charge	Species	Mass Error (ppm)	%
525.88164	525.13325	-4		-	1.14
550.12908	550.37984	-4		-	1.15
575.66102	575.91153	-4	$[cage + (Et_4N)(HNEt_3)]^{4-}$	1.81	4.28
582.66875	583.16930	-4	$[cage + (Et_4N)_2]^{4-}$	1.63	14.67
641.90823	642.15815	-4		-	7.6
575.38082	575.63061	-4		-	4.5
743.22912	743.56421	-3		-	2.53
765.72434	766.22586	-2		-	1.88
810.93427	811.22759	-3	$[cage + (Et_4N)_2(HNEt_3)]^{3-}$	1.59	4.27
820.27674	820.94461	-3	$[cage + (Et_4N)_3]^{3-}$	0.00	44.49
942.31837	942.98549	-3		-	3.02
958.34956	959.01697	-3		-	7.03
1266.34775	1267.34243	-2	$[cage +(Et_4N)(HNEt_3)Na_2]^{2-}$ + DMSO + 2MeCN + H_2O*	-15.05	0.06
1281.42767	1281.92988	-2	$[cage + (Et_4N)_3(HNEt_3)]^{2-}$ *	-40.04	0.5
1295.49463	1295.99949	-2	$[cage + (Et_4N)_4]^{2-}$	0.00	0.77
1316.01536	1317.01879	-2	$[cage + (Et_4N)_4 + MeCN]^{2-}$	5.67	0.83
1335.00905	1335.51102	-2		-	1.27

* indicates assignment of species, where large mass error may be attributable to overlapping peaks in the mass spectrum.

3. Analysis of $(NEt_4)_4(HNEt_3)_4[(PhSi)_6(ctc)_4]$·solvate soaked in CsBr

Figure S11 shows the full negative mode, high resolution ESI mass spectrum of the sample obtained for crystals of the compound that had been immersed in an aqueous CsBr solution then dissolved in dimethylformamide and diluted with acetonitrile. Overlapping isotopic profiles of the cage with caesium and tetraethylammonium cations reflect the similarity in the mass of Cs^+ and NEt_4^+.

Table S3 lists the dominant isotopologues in the full spectrum. The relative intensities of the base peaks within each of the isotopologue series are indicated as their percentage contribution to the sum of the intensities of the base peaks in each of the isotopologue series. The error (in ppm) for each species is calculated based upon the monoisotopic peak for each isotopologue series.

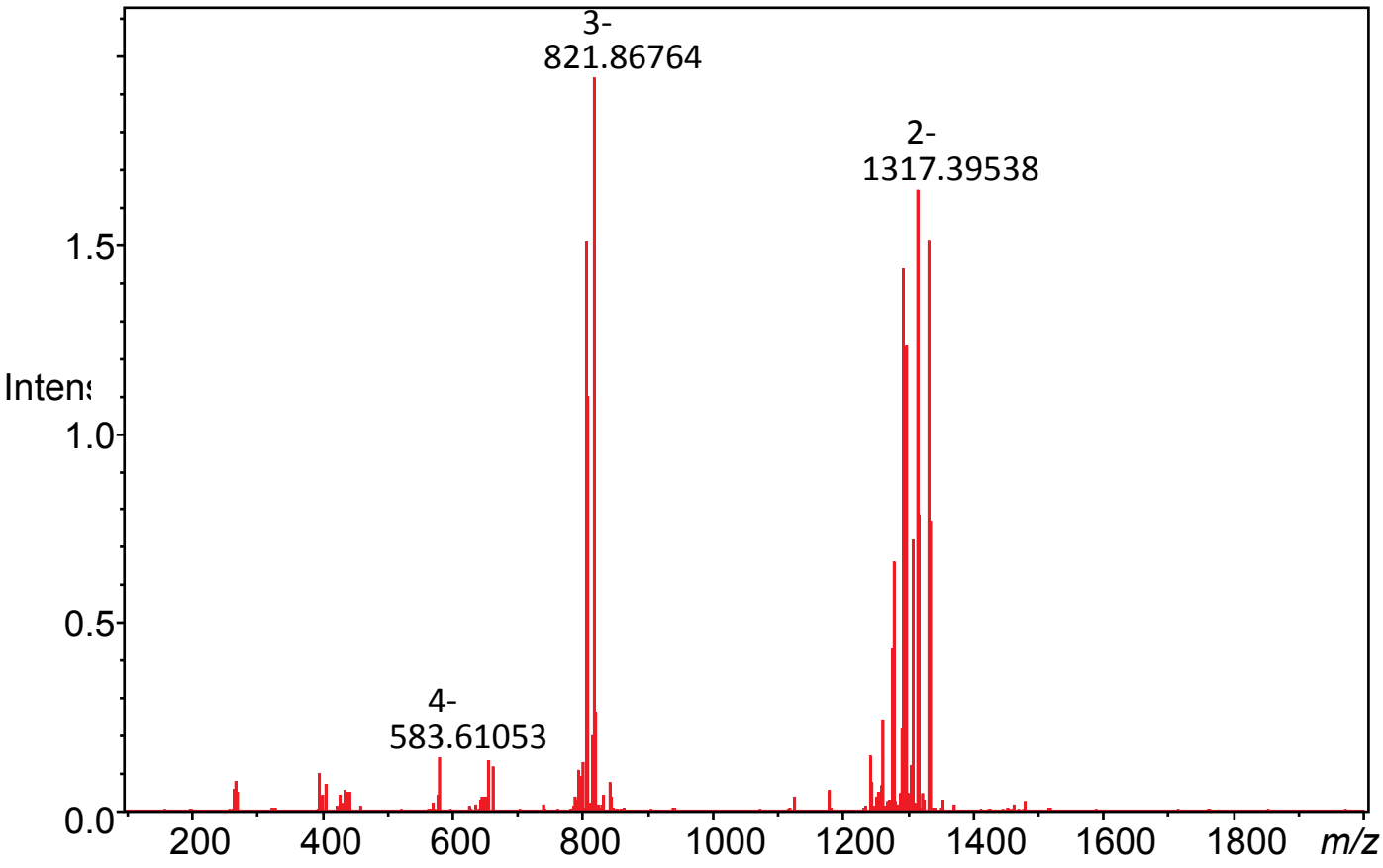

Figure S11. Full negative mode mass spectrum of the crystals soaked in aqueous CsBr solution followed by dissolution in DMF and dilution with MeCN.

Table S3. Selected negative ionisation mode mass spectrum data for crystals soaked in aqueous CsBr solution followed by dissolution in DMF and dilution with MeCN.

m/z **(monoisotopic peak)**	***m/z*** **(base peak)**	**Charge**	**Species**	**Mass Error (ppm)**	**%**
583.35201	583.60465	-4	$[cage + (Et_4N)Cs]^{4-}$	-3.88	1.1
658.18834	658.68071	-4		-	1
666.72091	667.21334	-4		-	0.9
804.49608	805.16206	-3		-	1
809.81919	810.48446	-3	$[cage + (Et_4N)CsNa + DMF]^{3-}$	-0.62	11.4
820.27674	820.61027	-3	$[cage + (Et_4N)_3]^{3-}$	0.00	3.4
821.18882	821.85240	-3	$[cage + (Et_4N)_2Cs]^{3-}$	-3.92	14.8
822.10659	822.43943	-3	$[cage + (Et_4N)Cs_2]^{3-}$	-0.90	2.4
845.54184	845.87536	-3	$[cage + (Et_4N)_2Cs + DMF]^{3-}$	-1.32	0.6
1181.27721	1182.27765	-2		-	0.4
1244.32811	1245.30638	-2	$[cage + (Et_4N)Na_3 + 3DMF]^{2-}$	7.27	1.1
1254.79724	1255.77383	-2	$[cage + (HNEt_3)_3Cs]^{2-}$ *	-18.63	0.4
1262.75663	1263.27346	-2	$[cage + (Et_4N)CsNa_2 + 2DMF]^{2-}$	4.83	1.9
1278.47421	1279.44904	-2	$[cage + (Et_4N)_3Na + DMF]^{2-}$ *	29.80	3.3
1279.94562	1280.81415	-2	$[cage + (Et_4N)_2CsNa + DMF]^{2-}$ *	106.71	5
1291.31199	1292.30828	-2		-	1.7
1295.49463	1296.48253	-2	$[cage + (Et_4N)_4]^{2-}$	0.00	10.9
1299.27040	1300.27425	-2	$[cage + (Et_4N)CsNa_2 + 3DMF]^{2-}$	-5.01	9.4
1308.35264	1309.34288	-2	$[cage + (Et_4N)_2(HNEt_3)_2 + 2MeCN]^{2-}$ *	-104.88	5.5
1316.35977	1317.34789	-2	$[cage + (Et_4N)(HNEt_3)_2Na + 2DMF + MeCN + H_2O]^{2-}$ *	-68.35	12.5
1333.42580	1334.41156	-2	$[cage + (Et_4N)_3Cs + DMF]^{2-}$ *	23.89	11.5

* indicates assignment of species, where large mass error may be attributable to overlapping peaks in the mass spectrum.

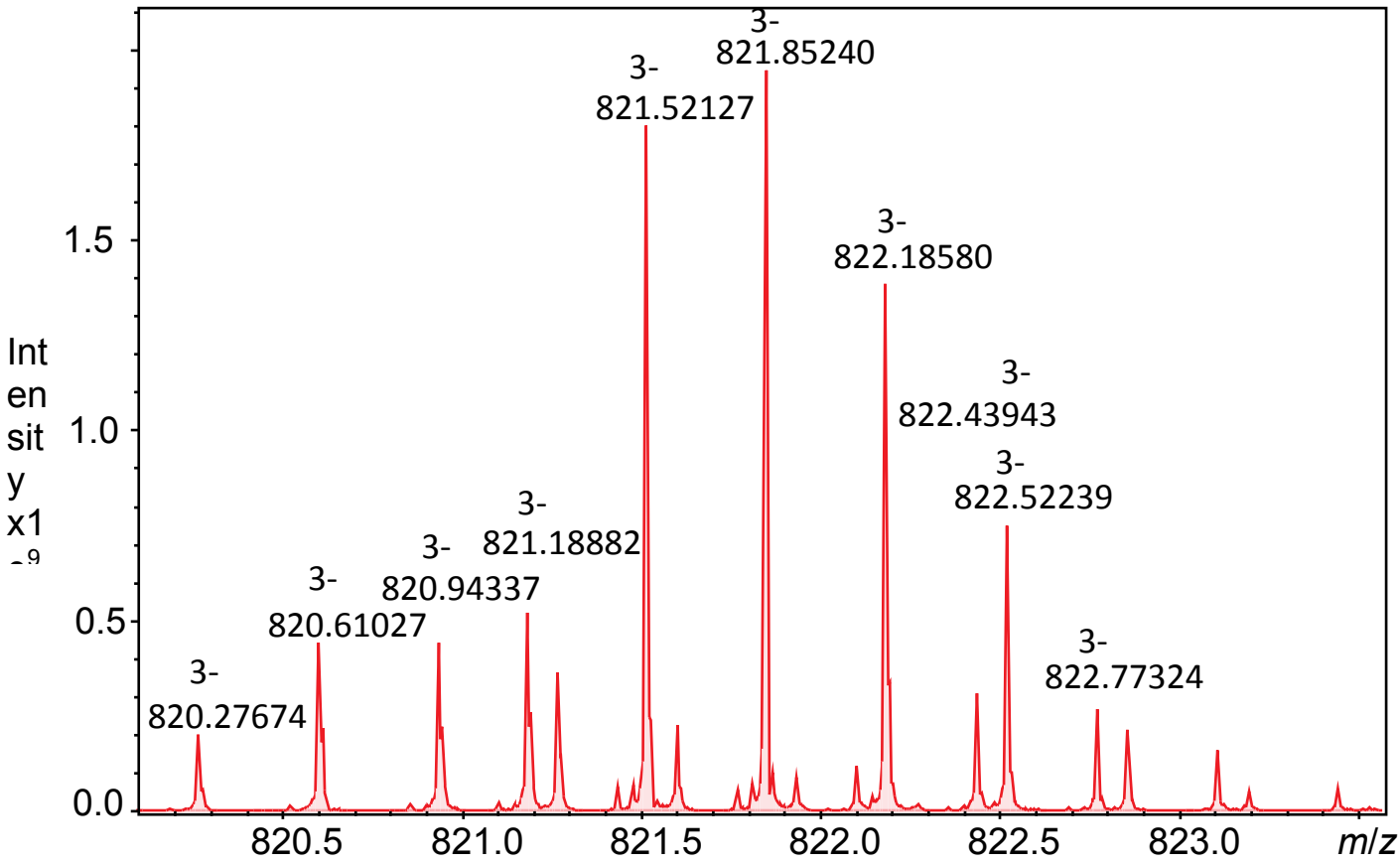

Figure S12. Shows three overlapping isotopic profiles of [cage + $(Et_4N)_3]^{3-}$ at *m/z* 820.61027, [cage + $(Et_4N)_2(Cs)]^{3-}$ (most abundant) at *m/z* 821.85240 and [cage + $(Et_4N)(Cs)_2]^{3-}$ at *m/z* 822.

S9. Infra-red spectroscopy

Infra-red spectrum $(NEt_4)_4(HNEt_3)_4[(PhSi)_6(ctc)_4]Br_2$·solvate (pressed KBr disc)

IR(KBr) cm^{-1}: 3431, 3065, 3025, 2984, 2918, 2854, 1619, 1498, 1384, 1277, 1254, 1171, 1119, 938, 890, 858, 738, 704, 672, 612, 521

The infra-red spectrum of $(NEt_4)_4(HNEt_3)_4[(PhSi)_6(ctc)_4]Br_2$·solvate (pressed KBr disc) is presented in Figure S16.

Infra-red spectrum of crystal after soaking in aqueous CsBr (pressed KBr disc)

IR(KBr) cm^{-1}: 3427, 3065, 3024, 2982, 2925, 2860, 1658, 1619, 1498, 1384, 1277, 1253, 1170, 1117, 1000, 937, 890, 858, 738, 704, 610, 521.

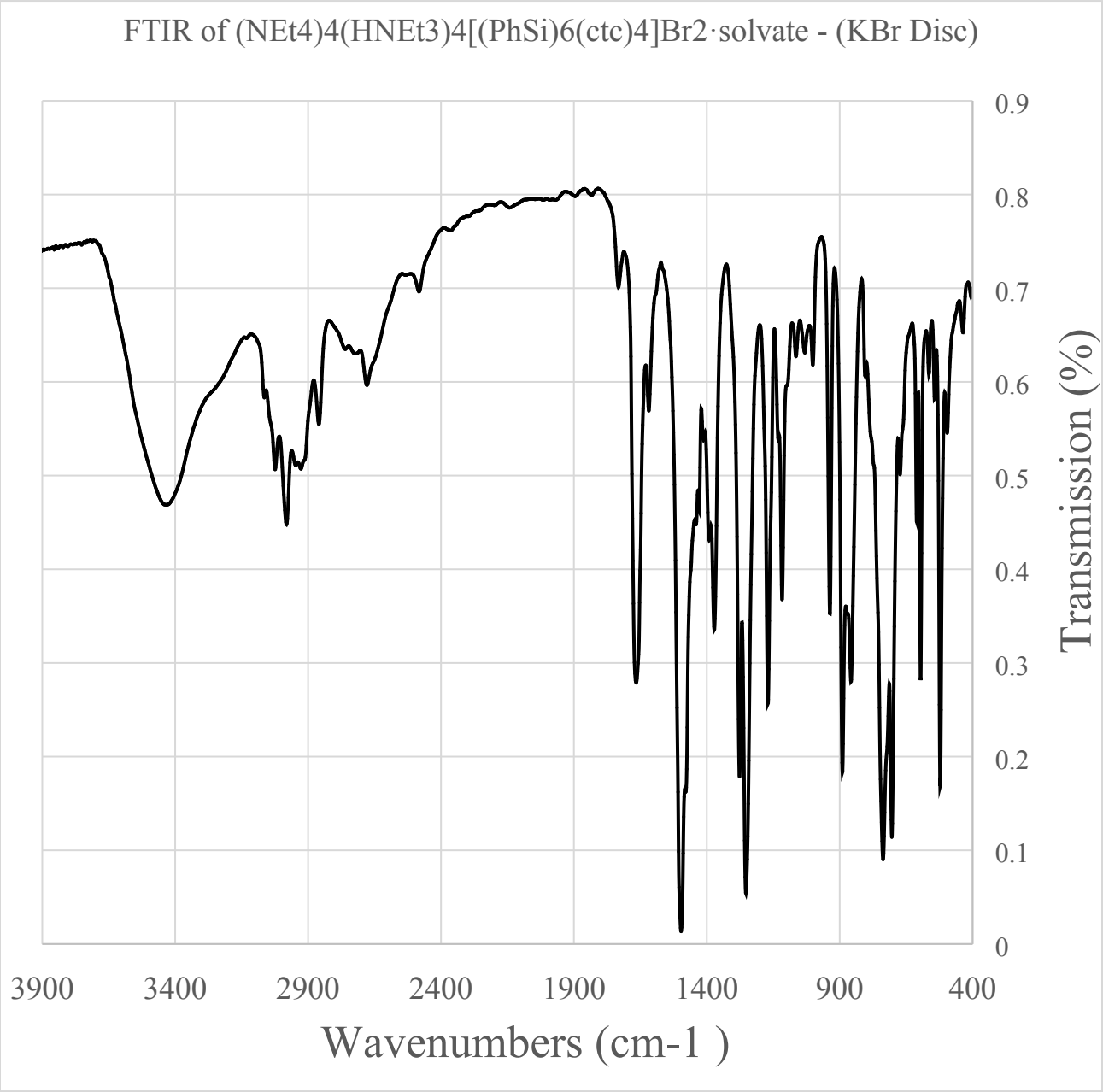

Figure S13. Infrared spectrum of $(NEt_4)_4(HNEt_3)_4[(PhSi)_6(ctc)_4]Br_2$·solvate (pressed KBr disc).

S10. References for ESI

1. A. Spek, *Acta Cryst. Sect. C*, 2015, **71**, 9-18

2. A. Spek, *Acta Cryst. Sect. D*, 2009, **65**, 148-155.

3. G. Sheldrick, *Acta Cryst Sect. A*, 2015, **71**, 3-8

4. G. Sheldrick, *Acta Cryst. Sect. C*, 2015, **71**, 3-8

5. L. Farrugia, *J. Appl. Cryst.*, 2012, **45**, 849-854.

6. O. V. Dolomanov, L. J. Bourhis, R.J. Gildea, J. A. K. Howard and H. Puschmann, *J. Appl. Cryst.* 2009, **42**, 339-341.